JVI Journals.ASM.org

HIV-1 Envelope Glycoprotein Trimers Display Open Quaternary Conformation When Bound to the gp41 Membrane-Proximal External-Region-Directed Broadly Neutralizing Antibody Z13e1

Audray K. Harris, Alberto Bartesaghi, Jacqueline L. S. Milne, Sriram Subramaniam

Laboratory of Cell Biology, Center for Cancer Research, National Cancer Institute, NIH, Bethesda, Maryland, USA

We describe cryo-electron microscopic studies of the interaction between the ectodomain of the trimeric HIV-1 envelope glycoprotein (Env) and Z13e1, a broadly neutralizing antibody that targets the membrane-proximal external region (MPER) of the gp41 subunit. We show that Z13e1-bound Env displays an open quaternary conformation similar to the CD4-bound conformation. Our results support the idea that MPER-directed antibodies, such as Z13e1, block viral entry by interacting with Env at a step after CD4 activation.

The HIV-1 envelope glycoprotein (Env) is a key target for neutralizing antibodies that can bind to the virus and thus prevent entry into target cells (1–3). Functional Env is a trimer, with each protomer composed of a heterodimer of gp120 and gp41 (4). The three protomers associate to form a "spike" on the surface of the viral membrane (5). Cryo-electron tomographic studies have provided molecular structures of a variety of trimeric envelope glycoproteins, both as spikes displayed on intact viruses and as soluble ectodomains (5–9). These studies have shown that when trimeric HIV-1 Env is in an unliganded state or when bound to the neutralizing antibody VRC01, it exists in a "closed" conformation, with the V1/V2 loops located close to the apex of the spike. When trimeric HIV-1 Env is bound to the neutralizing antibody b12, the trimer displays a partially open conformation with only a slight rearrangement of each gp120 monomer. In contrast, when bound to soluble CD4 or to coreceptor binding site reagents, such as the monoclonal antibody 17b, both soluble and native forms of trimeric HIV-1 Env display a fully open quaternary conformation. In this open state, the three gp120 monomers display a major structural rearrangement relative to their conformation in the closed state, involving large rotations of each gp120 monomer (5, 7). Whether these changes in quaternary conformation to open and partially open states are induced by antibody binding or whether the trimeric spikes are in a dynamic equilibrium between closed, partially open, or open states, with ligand binding shifting the relative populations, is not yet understood.

Atomic-resolution structures are available for the complexes formed between the monomeric gp120 subunit of Env and a variety of antibodies that target the CD4 binding site region. Much less structural information is available for complexes formed between the gp41 subunit and gp41-targeted neutralizing antibodies. No atomic-resolution structural models are available for trimeric gp41 in the prefusion state. However, the region of the gp41 ectodomain that is closest to the viral membrane, the membrane-proximal external region (MPER), has been identified as a key antigenic site that is the target of a number of neutralizing antibodies, such as 2F5, 4E10, 10E8, and Z13e1, with atomic structures available for the complexes formed between Fab fragments from each of these antibodies and the relevant peptide epitopes on gp41 (10–13). However, no structural information is available for the complex formed between MPER-binding antibodies and gp41 either as a protomer or in the context of intact trimeric HIV-1 Env. Here, we present cryo-electron microscopic studies of the complex formed between the Fab fragment of the MPER antibody Z13e1 and trimeric SOSIP gp140, which is a cleaved, solubilized version of the ectodomain of trimeric HIV-1 Env (Fig. 1A) (22). In previous studies, we demonstrated that this soluble gp140 trimer displays the same closed and open quaternary conformations as native trimeric Env. Moreover, because the linear gp41 epitope recognized by Z13e1 closely overlaps the binding sites of other broadly neutralizing MPER antibodies, such as 10E8, 4E10, and 2F5, the structural information derived from studies of the complex between trimeric gp140 and Z13e1 will likely also provide useful general insights into the interaction between Env and the other MPER antibodies.

We prepared frozen-hydrated specimens of soluble gp140 trimers incubated with Z13e1 Fab fragments and recorded projection images in a Titan Krios electron microscope equipped for operation at liquid nitrogen temperatures. Two-dimensional (2D) projection micrographs (Fig. 1B and C) and class averages (Fig. 1D and E) from individual gp140 molecular complexes demonstrate the presence of additional density from bound Fab in images recorded from the Z13e1-treated trimers compared to images from unliganded trimers. The density map of the complex, at a resolution of 18.5 Å, shows that Z13e1 binds at the base of the soluble Env trimer, with the bound Fab oriented roughly perpendicular to the central 3-fold axis (Fig. 2). Superposition of the structure of the Env-Z13e1 complex with that of native unliganded trimeric Env provides spatial context of the bound Z13e1 Fab relative to the viral membrane (Fig. 2K). If the location of Z13e1 binding to native Env is similar to the Z13e1 binding location on the soluble gp140 trimer, the footprint of the bound Fab fragment is expected to be above the plane of the viral membrane, as indicated in Fig. 2K. Further, the approximately horizontal orienta-

Received 3 December 2012 **Accepted** 9 April 2013
Published ahead of print 17 April 2013
Address correspondence to Sriram Subramaniam, ss1@nih.gov.

doi:10.1128/JVI.03284-12

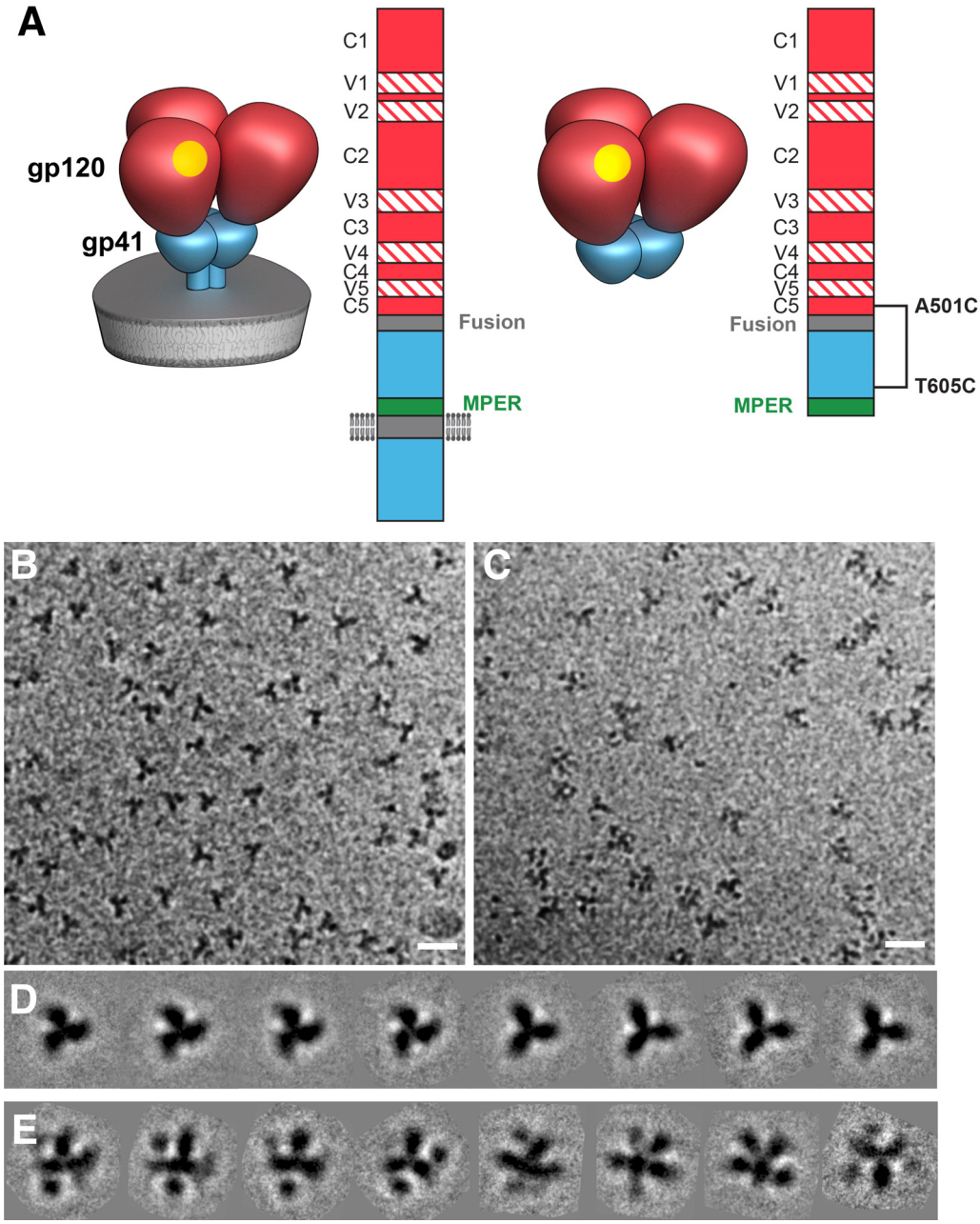

FIG 1 Cryo-electron microscopy of soluble gp140 trimers. (A) Schematic illustrating the arrangement, in the primary sequence of Env, of the constant (C1-C5) and variable (V1-V5) regions of gp120 and the MPER and transmembrane domains of gp41. The soluble gp140 construct (right) used in our studies includes gp120 and the entire ectodomain of gp41, with a size of ~20 kDa. Representations of the quaternary structures of full-length and soluble trimeric Env are shown alongside the schematic of the primary sequence, indicating the relative locations of gp120 (in red), gp41 (in blue), and the CD4 binding site (yellow). The soluble gp140 constructs include an engineered disulfide bond between residue 501 in gp120 and residue 605 in gp41. (B and C) Representative projection cryo-EM images at 80 kV of unliganded (B) or Z13e1 Fab-bound (C) KNH1144 SOSIP gp140 trimers. Scale bars = 20 nm. SOSIP gp140 trimers (6) were incubated on ice for 1 h with a 6-fold molar excess of Fab Z13e1 (~3.9 mg/ml), and specimens for cryo-electron microscopy were prepared as described previously (7). Images were collected on a Titan Krios electron microscope (FEI Company, Hillsboro, OR) equipped for operation at liquid nitrogen temperatures and operated at 80 kV. Five hundred eighty-three images were recorded using a 4,096 × 4,096 charge-coupled-device (CCD) camera (Gatan Inc., Warrendale, PA) at a pixel size of 1.35 Å and with defocus values ranging from ~1.3 to ~2.9 μm, at doses ranging from ~10 to 20 e−/Å^2. Micrographs were initially screened for astigmatism and/or drift, and those that showed significant problems were discarded from the analysis. From the remaining images, 7,050 individual particles were manually picked and extracted using a box size of 184 by 184 pixels. Contrast transfer function (CTF) parameters were estimated for each micrograph, and particle stacks were phase flipped before being subjected to 2D classification and 3D refinement using the software program EMAN (20). (D and E) Reference-free 2D class averages calculated from unliganded (D) or Z13e1-bound (E) gp140 trimers. The presence of the bound Z13e1 can be seen as the extra density not observed in unliganded gp140 trimers.

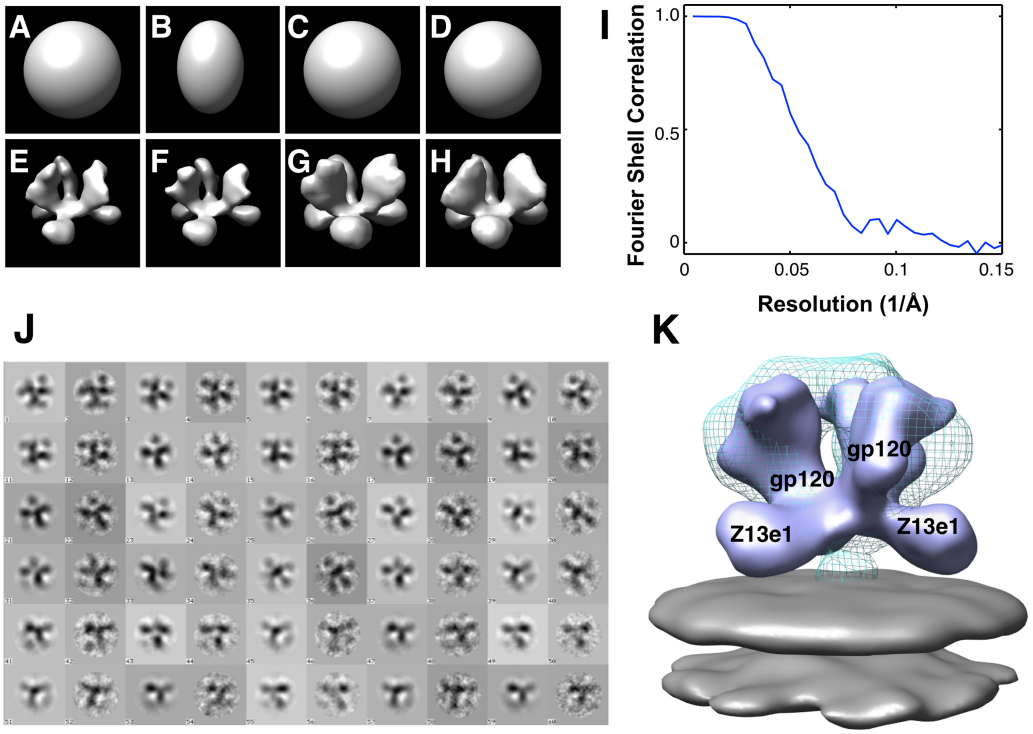

FIG 2 Refinement of the structure of the Z13e1-Env complex and comparison with the 3D structure of native Env. (A to H) Starting with unstructured Gaussian blobs as initial models, progressive steps in refinement with CTF-corrected phase-flipped images were carried out in the environment of the image-processing program EMAN (20). Starting models are shown in panels A to D, and the corresponding final models are shown in the same sequence in panels E to H. Gaussian blobs with different elongations in the perpendicular axis (panels A and B, with 1 and 2 times the elongation in the in-plane axes, respectively) were used as starting models in order to study the effect of initial model bias. For these experiments, the particle stack was low-pass filtered to 20 Å and binned by a factor of 2 to speed up the computations. Despite the difference in the shape of the starting models, the two instances produced similar reconstructions at low resolution, indicating robustness of the 3D refinement procedure. The binned particle stack was then split into two stacks: one containing the odd- and the other the even-number particles (3,525 images in each). Each stack was independently subjected to 3D refinement using the same Gaussian blob as the initial model and the same refinement parameters. These two independent refinements (panels C and D) also converged to the same 3D model, providing further proof of the validity of the 3D reconstruction. The full unbinned particle stack was then used to further refine the reconstruction using EMAN1's refine program with the following options: "mask = 70 pad = 256 hard = 25 classkeep = 0.8 classiter = 8 sym = C3 phasecls refine." The angular spacing for the rotational search was initially set to 8 degrees and then lowered to 5.7 degrees in the final refinement stages. The particle stack was low pass filtered to 20 Å during the coarser angular search stage and to 12 Å during the finer search. Refinement was stopped once the assignments of class memberships and angular orientations did not change significantly (after a total of 136 iterations). (I) Fourier shell correlation (FSC) plot obtained using all particles, computed using EMAN1's program eotest with the options "hard = 25 sym = c3 mask = 70 pad = 256 classkeep = 0.8 classiter = 8 fscmp," giving an estimated resolution of 18.5 Å as measured by the 0.5-cutoff FSC criteria. (J) Alternating gallery of reprojections of the refined 3D model (odd columns) and corresponding class averages obtained from the refinement procedure (even columns) is shown. (K) Superposition of the map of the Z13e1-Env complex (solid isosurface), produced using the software program UCSF Chimera (21), with the density map for native HIV-1 BaL trimeric Env (Electron Microscopy Data Bank identifier 5019 [EMDB ID 5019]) (cyan wire-mesh) (5). The Z13e1 Fab density is oriented roughly perpendicular to the trimeric 3-fold axis and is located above the plane of the viral membrane (gray).

tion of the Fab fragment relative to the plane of the bilayer membrane allows for the possibility that the other Fab arm of the antibody could potentially interact with the bilayer membrane, consistent with models of MPER antibody binding to the membrane prior to binding gp41 (14).

In order to obtain a molecular interpretation of the density map of the gp140-Z13e1 complex, we fitted atomic models for the structures of gp120 (from Protein Data Bank identifier 1GC1 [PDB ID 1GC1]) and the Z13e1 Fab-MPER peptide complex (PDB ID 3FN0) into the map. As expected, the fitting of Z13e1 Fab localizes the MPER peptide close to the gp140 trimer base and near the 3-fold axis of the trimer (Fig. 3). Surprisingly, the fit of gp120 shows that the conformation of each gp120 protomer is such that the V1/V2 loop region is pointed away from the center of the trimer (Fig. 3 and 4). This quaternary conformation of trimeric gp140 closely matches the CD4-bound conformation of both soluble gp140 and native trimeric HIV-1 Env, demonstrating that the arrangement of the three gp120 protomers in both soluble and membrane-bound versions of trimeric Env is directly influenced by the presence of Z13e1 at the MPER site. We have shown previously that trimeric Env bound to 17b, either in the absence or in the presence of soluble CD4, displays an open quaternary conformation similar to that seen with the binding of soluble CD4 alone (7). At the present resolution of these studies, the open quaternary conformations observed when CD4, 17b, or Z13e1 is bound to Env appear to display similar quaternary states of Env; it remains to be determined whether there are subtle differences between these states that reflect different stages of the entry process.

Our experiments thus show that Z13e1-bound trimeric Env displays an "open" quaternary conformation (Fig. 3 and 4), suggesting that events at the MPER domain are connected with the quaternary conformation of trimeric Env as a whole. Since the formation of the open quaternary conformation is associated with

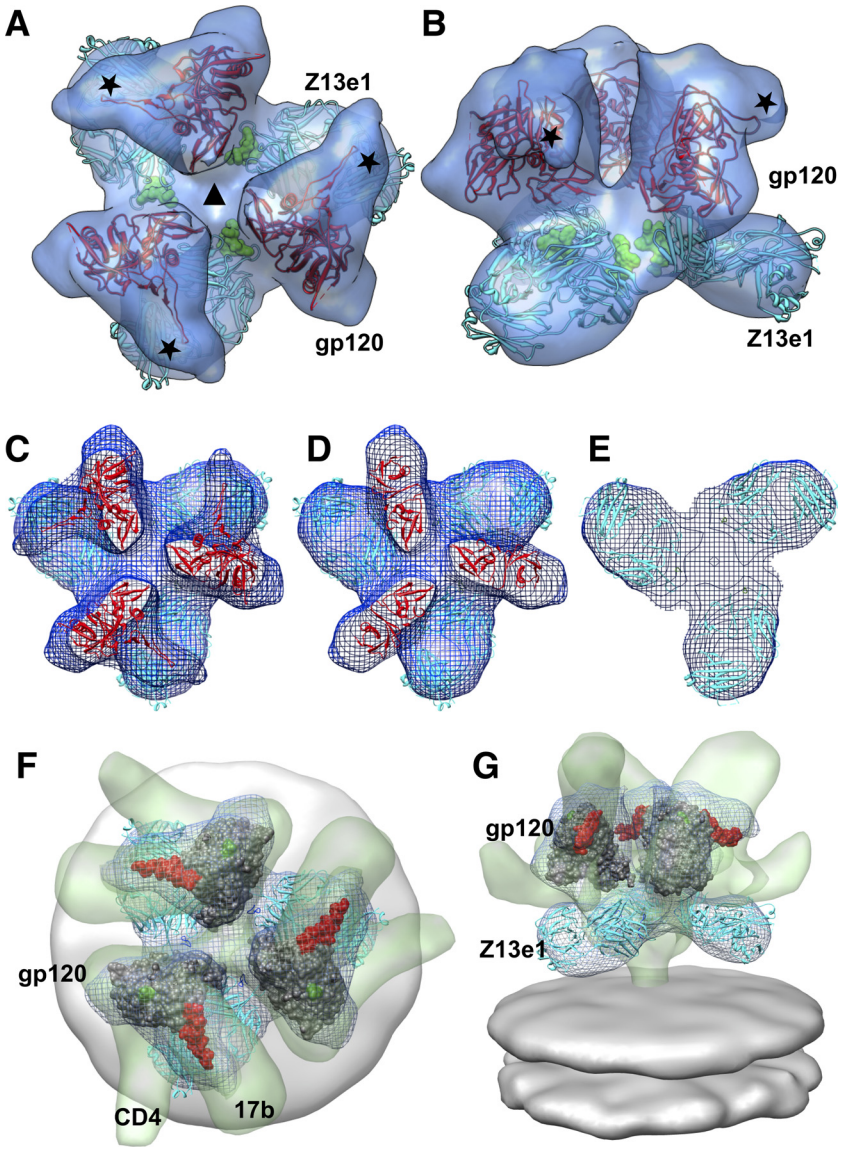

FIG 3 Molecular model for the Z13e1-Env complex. Top (A) or side (B) view of the density map (transparent isosurface), shown with docked coordinates for gp120 (PDB ID 1GC1; in red) and Fab Z13e1 (PDB ID 3FN0; in cyan). The MPER peptide epitope bound by Z13e1 is shown as a space-filling model (in green) and is located near the base of trimeric gp140. The asterisks mark the expected locations of the density for the V1/V2 loop region, which were truncated in the gp120 construct crystallized to obtain the gp120 structure reported in the 1GC1 coordinates. The gp120 and Z13e1 structures were docked into the map using automated fitting procedures implemented in the UCSF Chimera software package (21). (C to E) Selected slices through the reconstruction, with the map shown in wire mesh. (F and G) Comparison of quaternary state of trimeric gp120 in the Z13e1-bound state with that of sCD4/17b-bound Env complex (EMDB ID 5020), with both maps fit to the same coordinates for the gp120 trimer (PDB ID 3DNO). Top (F) or front (G) view is shown. The map of the Env/sCD4/17b complex is in transparent green, with CD4 and 17b Fab density protrusions labeled, and the Z13el map is in blue mesh; the gp120 core is shown in dark gray, with the stumps of the truncated V1/V2 and V3 loops shown in red and green, respectively. The Z13e1 Fab coordinates are cyan.

binding of ligands such as soluble CD4 and 17b, we conclude that there is a close coupling between changes in the quaternary arrangement of trimeric gp120 and the exposure of the gp41 MPER. Another implication of these findings is that the MPER region is accessible to Z13e1 in the activated state and not in the unliganded state. Our results are consistent with those of a number of studies that have suggested that binding of MPER site antibodies to virion and cell surface Env is enhanced by the presence of soluble CD4 (11, 15, 16). Taken together, all of these findings lead to a model for binding of MPER antibodies at a late stage in the HIV entry process, following CD4 binding and possibly after gp120 has bound cellular receptors such as CCR5 or CXCR4. This mode of binding may explain why we have not yet been able to obtain density maps that convincingly demonstrate binding of MPER antibodies, such as Z13e1 antibodies, to functional spikes on native HIV-1 virions.

The mechanism by which MPER-binding antibodies bind Env and block entry has remained a long-standing question in the HIV field. Our previous studies have suggested that CD4 binding site antibodies, such as VRC01 or b12, block entry by preventing formation of the open quaternary conformation (5, 7). Antibodies such as 17b are bound in the open quaternary conformation but

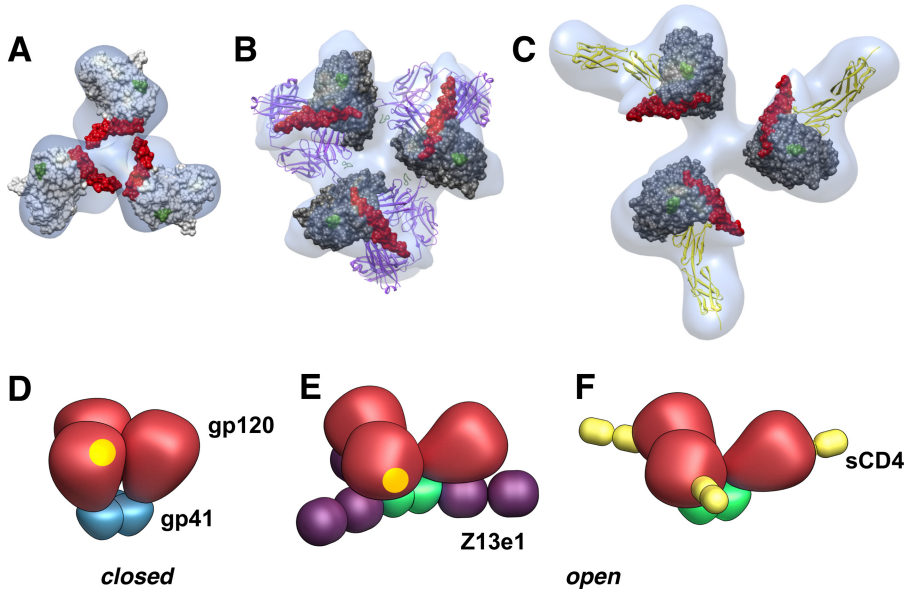

FIG 4 Comparison of quaternary states of trimeric gp120 in unliganded, Z13e1-bound and CD4-bound Env complexes. (A to C) Top views of maps and gp120 fits in an unliganded (A), Z13e1-bound (B), or sCD4-bound (C) state. Maps (transparent isosurfaces) are fitted with space-filling models of gp120 coordinates (PDB ID 1GC1), shown in light gray in the unliganded closed conformation (A) and dark gray in the Z13e1 and sCD4 open conformations (B and C). The truncated V1/V2 and V3 loops of gp120 from 1GC1 coordinates are red and green, respectively. The Z13e1 Fab coordinates from PDB ID 3FN0 are purple, while sCD4 coordinates from PDB ID 1GC1 are colored yellow. Maps of trimeric gp140 and sCD4-bound trimeric gp140 are from our previously published maps (EMDB ID 5320 and EMDB ID 5321). (D to F) Schematic representations of the conformations of trimeric gp120 in unliganded, Z13e1-bound, and sCD4-bound states, corresponding to the docked structure in panels A, B, and C, respectively. The CD4 binding site is marked as a yellow patch on gp120 (red); the gp41 portions are colored blue and green in the closed and open states, respectively.

appear to block entry by virtue of their location at the apex of the spike, interfering with virus-cell contact. The action of MPER antibodies is at a distance from the site of virus-cell contact, but it has been shown (11, 16–18) that at least some antibodies, such as 2F5, 4E10, and Z13e1, are capable of binding membrane surfaces even in the absence of Env. While it is formally possible that Z13e1 may work by binding to the closed conformation and pretriggering the open conformation of the spike or that Z13e1 captures a conformation of trimeric Env that is sampled by thermal fluctuations from the closed conformation, we favor the possibility that Z13e1 functions in HIV neutralization by binding to the viral membrane surface first prior to binding Env. Prebinding would be expected to increase the local concentration of antibodies near the base of trimeric Env, allowing them to bind to gp41 following Env activation by CD4. HIV entry into target cells requires formation of the entry claw by clustering of Env at the virus-cell contact zone (19) and the subsequent fusion between virus and cell membranes (4). The location of Z13e1 at the base of the spike, close to the viral membrane, suggests that this site could be sterically restricted for access to MPER-directed antibodies after formation of the entry claw, especially given the close (~10-nm) spacing of the neighboring "teeth" of the claw. We propose that the "attach and attack" mode of binding by Z13e1 in the immediate vicinity of the viral membrane is thus likely to inhibit both formation of the entry claw and the changes in membrane curvature required for fusion, providing a mechanism for entry inhibition distinct from that mediated by neutralizing antibodies such as VRC01 or b12, which target the gp120 component of Env.

ACKNOWLEDGMENTS

This work was supported by the Center for Cancer Research at the National Cancer Institute, NIH, and the IATAP program at NIH.

We thank Lesley Earl, Mario Borgnia, and Alan Merk for many helpful discussions, Kenneth Kang and William Olson for providing soluble KNH1144 gp140 trimers, Robert Pejchal, Dennis Burton, and Ian Wilson for providing Z13e1 Fab fragments, Ethan Tyler for assistance with figures, and staff at the Biowulf Linux cluster at the National Institutes of Health (Bethesda, MD) (http://biowulf.nih.gov).

REFERENCES

1. **Wu X, Yang ZY, Li Y, Hogerkorp CM, Schief WR, Seaman MS, Zhou T, Schmidt SD, Wu L, Xu L, Longo NS, McKee K, O'Dell S, Louder MK, Wycuff DL, Feng Y, Nason M, Doria-Rose N, Connors M, Kwong PD, Roederer M, Wyatt RT, Nabel GJ, Mascola JR.** 2010. Rational design of envelope identifies broadly neutralizing human monoclonal antibodies to HIV-1. Science **329**:856–861.
2. **Wu X, Zhou T, Zhu J, Zhang B, Georgiev I, Wang C, Chen X, Longo NS, Louder M, McKee K, O'Dell S, Perfetto S, Schmidt SD, Shi W, Wu L, Yang Y, Yang ZY, Yang Z, Zhang Z, Bonsignori M, Crump JA, Kapiga SH, Sam NE, Haynes BF, Simek M, Burton DR, Koff WC, Doria-Rose NA, Connors M, Mullikin JC, Nabel GJ, Roederer M, Shapiro L, Kwong PD, Mascola JR.** 2011. Focused evolution of HIV-1 neutralizing antibodies revealed by structures and deep sequencing. Science **333**:1593–1602.
3. **Zhou T, Georgiev I, Wu X, Yang ZY, Dai K, Finzi A, Kwon YD, Scheid JF, Shi W, Xu L, Yang Y, Zhu J, Nussenzweig MC, Sodroski J, Shapiro L, Nabel GJ, Mascola JR, Kwong PD.** 2010. Structural basis for broad and potent neutralization of HIV-1 by antibody VRC01. Science **329**:811–817.
4. **Gallo SA, Finnegan CM, Viard M, Raviv Y, Dimitrov A, Rawat SS, Puri A, Durell S, Blumenthal R.** 2003. The HIV Env-mediated fusion reaction. Biochim. Biophys. Acta **1614**:36–50.
5. **Liu J, Bartesaghi A, Borgnia MJ, Sapiro G, Subramaniam S.** 2008. Molecular architecture of native HIV-1 gp120 trimers. Nature **455**:109–113.
6. **Harris A, Borgnia MJ, Shi D, Bartesaghi A, He H, Pejchal R, Kang YK, Depetris R, Marozsan AJ, Sanders RW, Klasse PJ, Milne JL, Wilson IA, Olson WC, Moore JP, Subramaniam S.** 2011. Trimeric HIV-1 glycoprotein gp140 immunogens and native HIV-1 envelope glycoproteins display

the same closed and open quaternary molecular architectures. Proc. Natl. Acad. Sci. U. S. A. **108**:11440–11445.
7. **Tran EE, Borgnia MJ, Kuybeda O, Schauder DM, Bartesaghi A, Frank GA, Sapiro G, Milne JL, Subramaniam S.** 2012. Structural mechanism of trimeric HIV-1 envelope glycoprotein activation. PLoS Pathog. **8**:e1002797. doi:10.1371/journal.ppat.1002797.
8. **White TA, Bartesaghi A, Borgnia MJ, de la Cruz MJ, Nandwani R, Hoxie JA, Bess JW, Lifson JD, Milne JL, Subramaniam S.** 2011. Three-dimensional structures of soluble CD4-bound states of trimeric simian immunodeficiency virus envelope glycoproteins determined by using cryo-electron tomography. J. Virol. **85**:12114–12123.
9. **White TA, Bartesaghi A, Borgnia MJ, Meyerson JR, de la Cruz MJ, Bess JW, Nandwani R, Hoxie JA, Lifson JD, Milne JL, Subramaniam S.** 2010. Molecular architectures of trimeric SIV and HIV-1 envelope glycoproteins on intact viruses: strain-dependent variation in quaternary structure. PLoS Pathog. **6**:e1001249. doi:10.1371/journal.ppat.1001249.
10. **Cardoso RM, Zwick MB, Stanfield RL, Kunert R, Binley JM, Katinger H, Burton DR, Wilson IA.** 2005. Broadly neutralizing anti-HIV antibody 4E10 recognizes a helical conformation of a highly conserved fusion-associated motif in gp41. Immunity **22**:163–173.
11. **Huang J, Ofek G, Laub L, Louder MK, Doria-Rose NA, Longo NS, Imamichi H, Bailer RT, Chakrabarti B, Sharma SK, Alam SM, Wang T, Yang Y, Zhang B, Migueles SA, Wyatt R, Haynes BF, Kwong PD, Mascola JR, Connors M.** 2012. Broad and potent neutralization of HIV-1 by a gp41-specific human antibody. Nature. doi:10.1038/nature11544.
12. **Ofek G, Tang M, Sambor A, Katinger H, Mascola JR, Wyatt R, Kwong PD.** 2004. Structure and mechanistic analysis of the anti-human immunodeficiency virus type 1 antibody 2F5 in complex with its gp41 epitope. J. Virol. **78**:10724–10737.
13. **Pejchal R, Gach JS, Brunel FM, Cardoso RM, Stanfield RL, Dawson PE, Burton DR, Zwick MB, Wilson IA.** 2009. A conformational switch in human immunodeficiency virus gp41 revealed by the structures of overlapping epitopes recognized by neutralizing antibodies. J. Virol. **83**:8451–8462.
14. **Alam SM, Morelli M, Dennison SM, Liao HX, Zhang R, Xia SM, Rits-Volloch S, Sun L, Harrison SC, Haynes BF, Chen B.** 2009. Role of HIV membrane in neutralization by two broadly neutralizing antibodies. Proc. Natl. Acad. Sci. U. S. A. **106**:20234–20239.
15. **Chakrabarti BK, Walker LM, Guenaga JF, Ghobbeh A, Poignard P, Burton DR, Wyatt RT.** 2011. Direct antibody access to the HIV-1 membrane-proximal external region positively correlates with neutralization sensitivity. J. Virol. **85**:8217–8226.
16. **Rathinakumar R, Dutta M, Zhu P, Johnson WE, Roux KH.** 2012. Binding of anti-membrane-proximal gp41 monoclonal antibodies to CD4-liganded and -unliganded human immunodeficiency virus type 1 and simian immunodeficiency virus virions. J. Virol. **86**:1820–1831.
17. **Phogat S, Svehla K, Tang M, Spadaccini A, Muller J, Mascola J, Berkower I, Wyatt R.** 2008. Analysis of the human immunodeficiency virus type 1 gp41 membrane proximal external region arrayed on hepatitis B surface antigen particles. Virology **373**:72–84.
18. **Song L, Sun ZY, Coleman KE, Zwick MB, Gach JS, Wang JH, Reinherz EL, Wagner G, Kim M.** 2009. Broadly neutralizing anti-HIV-1 antibodies disrupt a hinge-related function of gp41 at the membrane interface. Proc. Natl. Acad. Sci. U. S. A. **106**:9057–9062.
19. **Sougrat R, Bartesaghi A, Lifson JD, Bennett AE, Bess JW, Zabransky DJ, Subramaniam S.** 2007. Electron tomography of the contact between T cells and SIV/HIV-1: implications for viral entry. PLoS Pathog. **3**:e63. doi:10.1371/journal.ppat.0030063.
20. **Ludtke SJ, Baldwin PR, Chiu W.** 1999. EMAN: semiautomated software for high-resolution single-particle reconstructions. J. Struct. Biol. **128**:82–97.
21. **Pettersen EF, Goddard TD, Huang CC, Couch GS, Greenblatt DM, Meng EC, Ferrin TE.** 2004. UCSF Chimera—a visualization system for exploratory research and analysis. J. Comput. Chem. **25**:1605–1612.
22. **Sanders RW, Vesanen M, Schuelke N, Master A, Schiffner L, Kalyanaraman R, Paluch M, Berkhout B, Maddon PJ, Olson WC, Lu M, Moore JP.** 2002. Stabilization of the soluble, cleaved, trimeric form of the envelope glycoprotein complex of human immunodeficiency virus type 1. J. Virol. **76**:8875–8889.